Ore Geology Reviews 115 (2019) 103165

Contents lists available at ScienceDirect

Ore Geology Reviews

journal homepage: www.elsevier.com/locate/oregeorev

Genesis of the Guangshigou pegmatite-type uranium deposit in the North Qinling Orogenic Belt, China

Youwei Chen*, Ruizhong Hu, Xianwu Bi, Jincheng Luo

State Key Laboratory of Ore Deposit Geochemistry, Chinese Academy of Sciences, Guiyang 550081, China

ARTICLE INFO

Keywords:
Pegmatite-type uranium deposit
Assimilation and fractional crystallization
Partial melting
Northern Qingling orogeny of North China Block

ABSTRACT

The Guangshigou uranium deposit is an important pegmatite-type uranium deposit located in the North Qinling Orogenic Belt (NQB), China. The characteristics pertaining to its chronology, petrogenesis, and geodynamic setting remain unclear till date. In this study, we present systematic zircon U–Pb ages, Lu–Hf isotopic data, and mineral chemistry of uranium-rich biotite pegmatite dikes. In situ zircon U–Pb dating of the biotite pegmatite dikes yielded early Caledonian ages (422–417 Ma). The initial $^{176}Hf/^{177}Hf$ ratios of the zircons from the biotite pegmatites showed a narrow range (0.282378–0.282590), with εHf values ranging from −5.1 to 2.8 and Paleoproterozoic to Mesoproterozoic two-stage Hf model ages between 1723 and 1227 Ma. The bulk and mineral chemistries of the pegmatites also indicate that the pegmatite dikes were derived from low-degree partial melting of Qinling Group rocks with monazite as the residual mineral. Differences between the normal biotite pegmatite and the mineralized biotite pegmatite dikes with respect to mineralogy, texture, structure, and mineral chemistry indicate that the assimilation between the pegmatite dikes and the wall rock, may be the primary mechanism for the mineralization of the uranium, with the fractional crystallization process being another important mechanism. Amphibolite facies metamorphism, which was most likely caused by the exhumation of the subducted slab in the NQB, may have been a key factor in the genesis of the uranium-rich pegmatitic magma.

1. Introduction

Uranium deposits can be formed under various geological conditions, including under high-grade metamorphic conditions, plutonic, metasomatic, hydrothermal, and basin diagenesis, and in volcanic to sedimentary and superficial environments (Cuney, 2011). According to these geological processes, uranium ore deposits are divided into dozens of groups based on different criteria (Skirrow, 2009; Cuney, 2012; IAEA, 2018). In intrusive type uranium deposits, the mineralization is associated with high-temperature magmatic systems such as alaskite, pegmatite, and granite (Cuney, 2012; Fayek, 2013; Cuney and Kyser, 2015). The main U mineral in this group is typically magmatic uraninite (or uranothorite in some cases). The ore grades of this type of uranium deposits are usually low (0.01%–0.1%). However, the deposits can vary from several tons to hundreds of thousands of tons of uranium depending on the sizes of the intrusive bodies. The largest deposit of this type is the Rössing deposit in Namibia (Basson and Greenway, 2004; Kinnaird and Nex, 2007), which contains approximately 246,500 t of low-grade (300 ppm) metal uranium (Cuney and Kyser, 2015). Although rare such deposits have been mined, researchers are becoming only recently interested in this type of uranium deposits owing to their resource potential and the rapidly increasing demand for uranium resources(Austman and Ansdell, 2010; McKeough et al., 2013; Mercadier et al., 2013).

Intrusive type uranium deposits in China are primarily distributed in the Danfeng area of the North Qinling Orogenic Belt (NQB), the Longshoushan area in the southwest margin of the North China Block (NCB), and the Liaodong Peninsula in the northeastern segment of the North China Craton (Tang, 2002). Of these, the Guangshigou pegmatite-type uranium deposit in the Danfeng area has the best prospects and have been the most studied since the 1960s (Wan et al., 1992; Zeng and Jin,1994; Feng et al., 1996; Zuo et al.,2010; Sha et al., 2011; Chen et al., 2013, 2018). These studies have focused primarily on the whole-rock geochemical characteristics of the pegmatite and its relationship with granite. However, some of the metallogenic features remain controversial, including mineralization timing (391–437 Ma: Sha et al., 2011; Wang et al., 2018; Yuan et al., 2018), origin of the pegmatite (fractional crystallization of the Huichizi granite or direct partial

Abbreviations: AFGs, Alkali-feldspar granites; BMGs, Biotite monzonitic granites; MBPs, Mineralized biotite pegmatites; NBPs, Normal biotite pegmatites; NCB, North China Block; NQB, North Qinling Orogenic Belt

* Corresponding author.
E-mail address: chenyouwei@mail.gyig.ac.cn (Y. Chen).

https://doi.org/10.1016/j.oregeorev.2019.103165
Received 7 November 2018; Received in revised form 12 September 2019; Accepted 7 October 2019
Available online 09 October 2019
0169-1368/

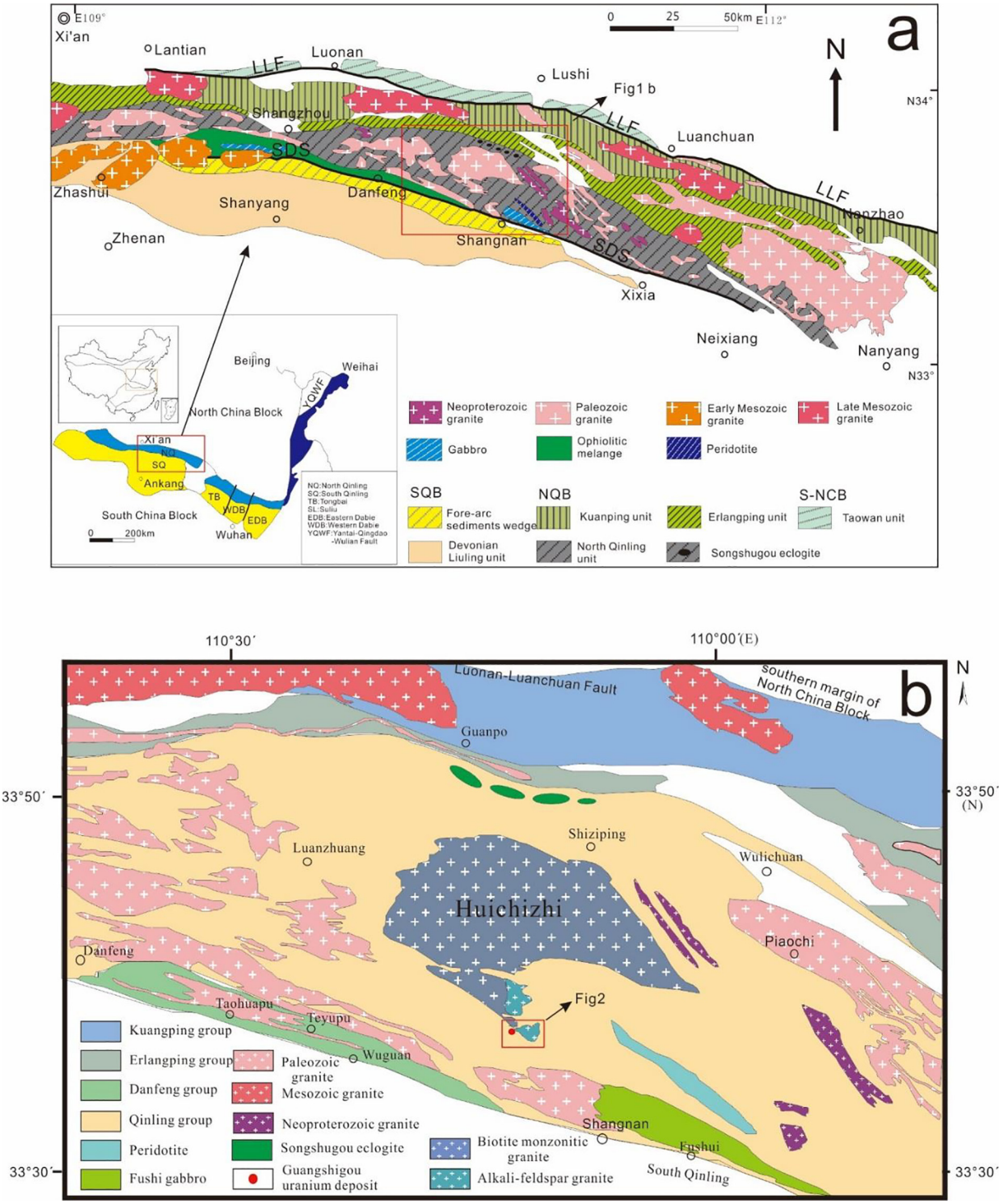

Fig. 1. Maps of the study area. (a) Schematic geological map of North Qinling orogenic belt. SDS: Shangdan suture; LLF: Luonan-Luanchuan Fault (modified after Dong et al., 2011; Wang et al., 2013b). (b) Geological map showing the Huichizi complex, North Qinling (modified after Zhang et al., 2013).

melting of the Qinling group, Chen et al., 2013; Feng et al., 1996, 2015; He et al., 2018; Sha et al., 2011; Wan et al., 1992; Wang et al., 2018; Zeng and Jin, 1994), and mechanism of uranium mineralization in the pegmatite (fractional crystallization or assimilation with wall rock: Wan et al., 1992; Zeng and Jin,1994, Chen et al., 2013; Yuan et al., 2018). In this study, we present systematic U–Pb ages and Lu–Hf isotopic data from zircons, and the mineral chemistry of the uranium-rich biotite pegmatite to ascertain the genesis of the Guangshigou uranium deposit.

2. Geological setting

The Qinling Orogenic Belt is one of the most important collision orogens in East Asia owing to its position at the convergence between South China Block and North China Block (Ratschbacher et al., 2003; Wu et al., 2009; Wu and Zheng, 2013). The NQB is an important section of the Qinling Orogenic Belt, bounded by the Luonan–Luanchuan Fault in the north and the Shangdan Suture in the south (Fig. 1a). The NQB is subdivided from north to south into several lithological units, including the Kuanping Group, Erlangping Group, Qinling Group, Songshugou

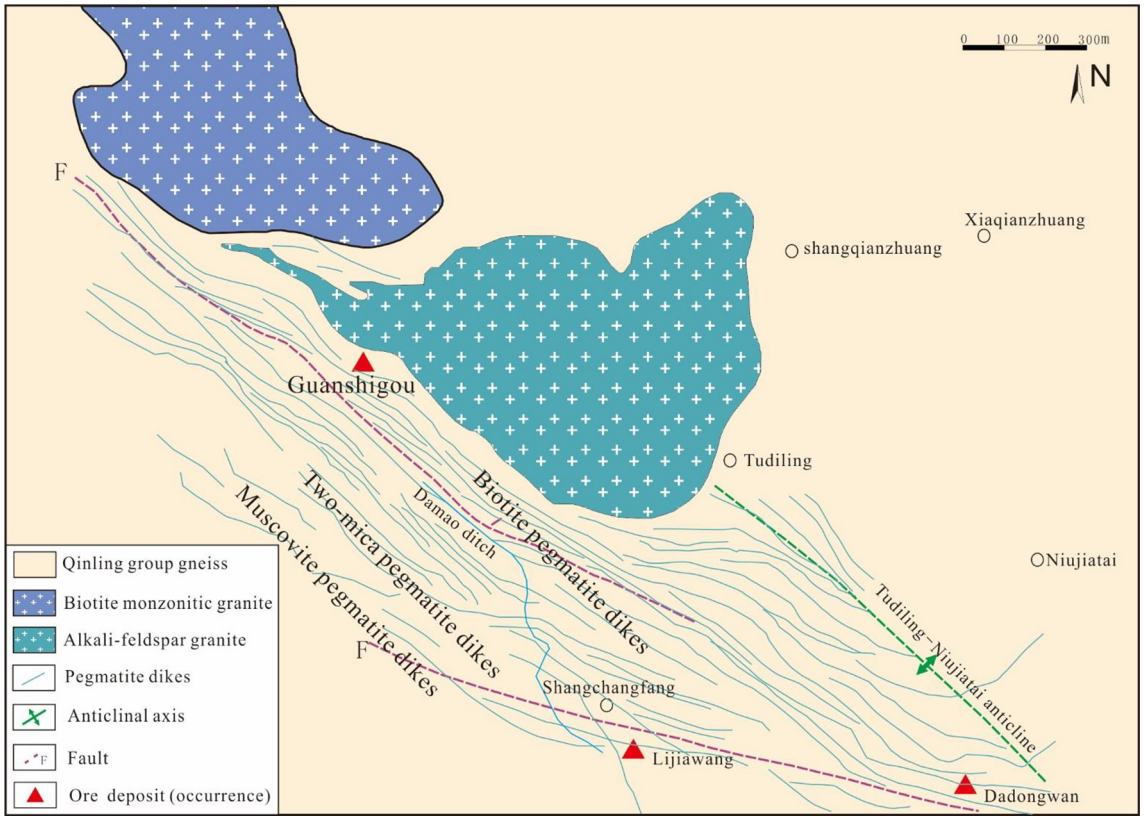

Fig. 2. Simplified geological map of Guangshigou uranium deposit (modified from Feng et al., 1996; Zuo et al., 2010).

Complex, and Danfeng Group, which are separated from each other by thrust faults or ductile shear zones (Dong et al., 2011; Zhai et al., 1998). The Guangshigou pegmatite-type uranium deposit intrudes into the Qinling Group and is hosted by the Huichizi granitic complex in the Danfeng area of the NQB (Fig. 1b).

The Qinling Group is the most important and oldest unit of the NQB. The depositional time-interval of the Qinling Group is controversial; however, in general, it is believed to be Paleoproterozoic (Zhang et al., 1988, Mesoproterozoic (Yang et al., 2003; Lu et al., 2006), and Neoproterozoic (Yang et al., 2010; Shi et al., 2013). The Qinling Group is composed of biotite–plagioclase and garnet–sillimanite gneisses, mica–quartz schists, graphite-bearing marbles, and amphibolites or garnet amphibolites with some eclogites (Ratschbacher et al., 2003). Of these, biotite–plagioclase gneiss is the most important rock type, and is the main wall rock of pegmatite dikes.

The Guangshigou uranium deposit is hosted by the Huichizi granite complex (Fig. 2). The orebodies are regular in morphology, and consist of pegmatite veins characterized by large amounts of biotite grains; A large number of pegmatite veins constitute low grade (average grade of ~400 ppm U) but bulk mass uranium deposit (No. 224 group of China National Nuclear Corporation, 2008). The ore mineral is dominated by uraninite, and the main gangue minerals include biotite, quartz, apatite, garnet, monazite, and zircon.

The Huichizi granitic complex is the largest I-type granite batholith in the NQB and covers an area of 340 km^2. It primarily consists of biotite monzonitic granites (BMG) and alkali-feldspar granites (AFG) (Fig. 1b). The BMG is generally gray and pale red in color with a medium- or coarse-grained texture. The mineral composition is mainly quartz (35%), K-feldspar (microcline; 15%–20%), plagioclase (30%–35%), and euhedral biotite (10%). The AFG appears pale red in color, has large mineral particles, and a simple mineral composition including quartz (35%), K-feldspar (microcline; 35%–40%), plagioclase (20%–25%), and a small amount of biotite (5%). Zircon laser ablation inductively coupled mass spectrometry (LA-ICPMS) data show that the BMG were intruded at 437–434 Ma and the AFG were intruded at 426–424 Ma (Qin et al., 2015; Chen et al., 2018).

Numerous pegmatite dikes are located south of the Huichizi granitic complex (Fig. 2). Three mineralogical types of pegmatite dikes occur in an obvious horizontal zoning in the granite and are classified as biotite pegmatite, two-mica pegmatite, and muscovite pegmatite based on the type and content of mica in them (Feng et al., 1996). The biotite pegmatites located around the *exo*-contact zone of the AFG are uranium-rich and contain uraninite grains; in contrast, the two-mica pegmatites and muscovite pegmatites are barren. However, only a minority of the biotite pegmatites can be regarded as mineralized (i.e. of economic significance) biotite pegmatites (MBP) owing to their high content of uraninite grains. To distinguish them from MBP, the biotite pegmatites that did not reach the desired mineralized level are regarded as normal biotite pegmatites (NBP) in this work.

3. Petrography

Fresh NBP and MBP rock samples were carefully selected from the outcrops and the mineralized drilling cores.

The NBP samples are gray to pink and have a coarse- to microcrystal granitic texture without mineral zoning (Fig. 3a, c). They possess a slightly heterogeneous composition, including microcline (40 vt.%), quartz (30 vt.%), plagioclase (20 vt.%), biotite (10 vt.%), and accessory minerals such as zircon, monazite, uraninite, and apatite. The uraninite grains are usually euhedral tabular and randomly distributed in or between the grains of quartz, feldspar, and biotite. The biotite grains are usually tiny, brown, subhedral tabular, and equally distributed.

The MBP samples show similar characteristics to the NBPs with respect to their mineral compositions; however, their textures and grain sizes are usually highly heterogeneous (Fig. 3b, d). Most MBPs are characterized by plumy aggregations of biotite with very small thin slices (Fig. 3d), while some are characterized by cores of smoky quartz and pink oligoclase. The plumy biotite grains are brown to dark brown,

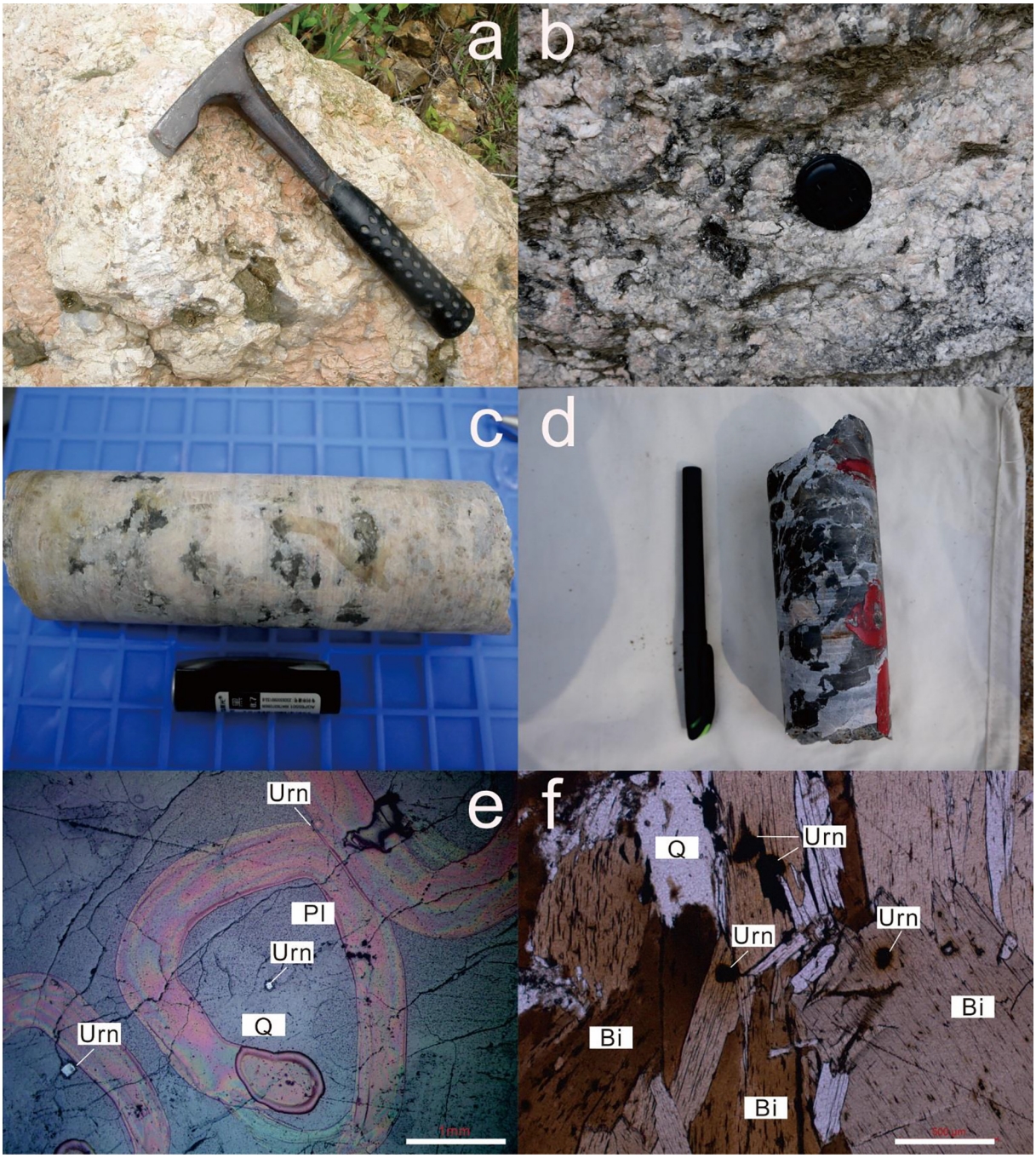

Fig. 3. Images of the biotite pegmatite dikes. (a) Field photograph. (b) Field photograph showing mineralization. (c) Photograph of a representative drill core sample, (d) Photograph of representative drill core sample with plumy biotite aggregations. (e) Photomicrograph of uraninite grains in the quartz and feldspar grains (reflected light). (f) Photomicrograph of uraninite grains in the plumy biotite (transmitted light). Abbreviations are: Bi: biotite; Pl: plagioclase; Q: quartz; Urn: uraninite.

small, subhedral to anhedral tabular, and deformed. Secondary muscovites are often distributed in the edges of the biotite. The MBPs usually intrude into the country rock of the Qinling Group, which is primarily composed of biotite–plagioclase gneiss. The MBPs characterized by plumy biotite clusters are most commonly developed at the contact zones between biotite pegmatite and biotite-plagioclase gneiss.

Uraninite grains in the MBPs are usually euhedral granular and set in the coarse-grained assemblage of biotite, quartz, and feldspar, commonly in conjunction zircon, and can reach up to 1 mm, with an average size of 100–200 μm (Fig. 3e, f); the differences in their location do not significantly influence their morphological or textural characteristics. Radioactive damage zones are always present at the uraninite grain boundaries, and are particularly common when the host minerals are biotite and feldspar (Fig. 3f). Aggregations of pyrite grains sometimes fringe the uraninite crystals, with smaller zircons crowded among them.

The zircon fractions in the pegmatites are usually interstitial to uraninite, feldspar, biotite, and quartz or are enclosed in quartz (Fig. 4a). Most of the zircon fractions are subhedral to euhedral, colorless to light brown, and semitransparent. The zircon crystals are prismatic in morphology and have well-developed {1 0 1} pyramids and {1 0 0} prisms, with axis lengths varying from 50 to 150 μm and elongation ratios of 1:1 to 2:1 (Fig. 4b, c).

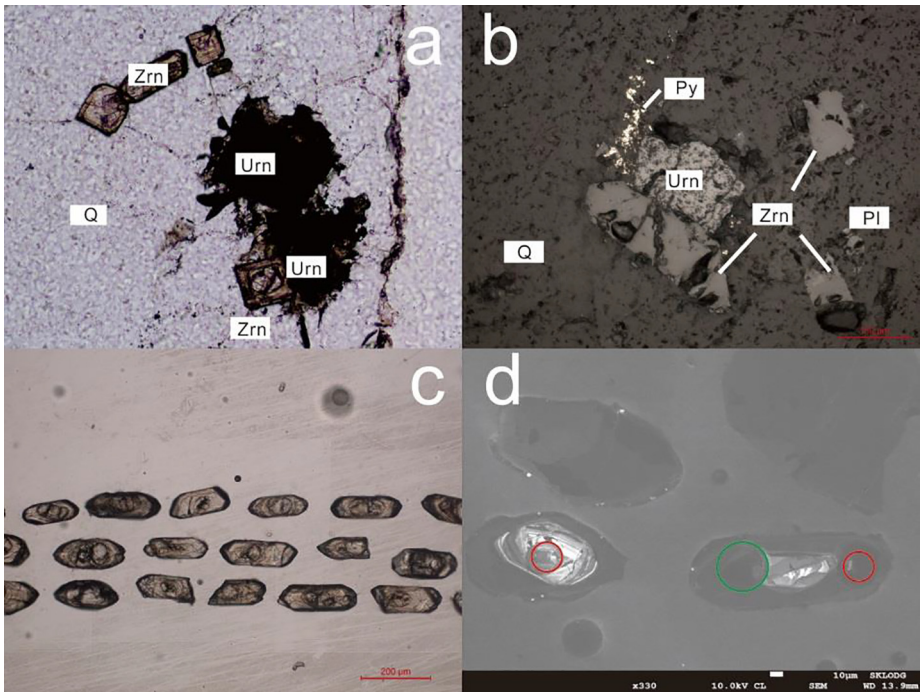

Fig. 4. Typical photomicrographs of the zircon fractions from the biotite pegmatites. The occurrence of zircon grains in the biotite pegmatites under transmitted light (a) and reflected light (b). (c) Morphology of selected zircon grains. (d) Cathodoluminescence (CL) images of representative zircon grains. Circles show the locations of U-Pb dating (red) and Hf isotopic ratio (green) analysis spots Abbreviations are: Zrn: zircon; Pl: plagioclase; Q: quartz; Urn: uraninite; Py: pyrite.

4. Sampling and analytical procedures

Eleven NBP and MBP samples were carefully selected for analyses based on their bulk major and trace element geochemical compositions. To ensure the representative uniformity of the samples, the total weight of each sample was no less than 5 kg for outcrop samples and 3 kg for drilling core samples.

Whole-rock element concentrations were analyzed at the State Key Laboratory of Ore Deposit Geochemistry, Chinese Academy of Sciences. The major elements were determined via X-ray fluorescence (XRF) on $LiBO_4$ fusion glass plates using an Axios (PW4400) XRF spectrometer. Certified standards were used for calibration. The trace elements in the granites were measured via inductively coupled plasma mass spectrometry (ICP-MS; PerkinElmer, ELAN DRC-e). The relative errors were < 5%, and the analytical errors for the major and trace elements were less than 1% and 10% (relative), respectively.

The mineral chemistry of biotite was ascertained using a JEOL JXA-8800 M electron probe micro-analyzer (EPMA) at the State Key Laboratory of Mineral Deposits Research in Nanjing University under the following conditions: an electron accelerating voltage of 25 kV, a beam size of 10 μm in diameter, and a beam current of 10 nA. The standards for the quantitative analysis included biotite, amphibole, apatite, and tugtupite obtained from the American National Standards Bureau. We calibrated and tested the elemental contents of Si, Al, Mg, K, Ti, and Fe using the biotite standard, contents of Ca, Mn, and Na against the amphibole standard, F content against the apatite standard, and the Cl content using the tugtupite standard. The EPMA data for feldspars were determined at the Analytical Laboratory of Beijing Research Institute of Uranium Geology on the JEOL JXA-8100 EPMA. The measurements were performed using the wavelength dispersive spectrometers at 20 kV, 50nA, and 10–100-s peak time. The conversion of raw counts to element concentrations was performed using the ZAF correction routine.

The U–Pb dating of the zircons was conducted using LA-ICP-MS at the State Key Laboratory of Ore Deposit Geochemistry, Institute of Geochemistry, Chinese Academy of Sciences, Guiyang. The GeoLasPro 193 nm ArF laser-ablation and Agilent 7700x ICP-MS (Agilent Technologies, Tokyo, Japan) systems were combined for the experiments. The ablation protocol employed a spot diameter of 44 μm at a 5-Hz repetition rate of 70 s. A blank run of 20–30 s (gas blank) was performed before a 30-s analysis of a sample. As the uranium contents could be high, pulse-analog cross-calibration for the ICP-MS was performed prior to the measurement of the U–Pb isotopes, similar to the method described in Zhao et al. (2014). The Agilent ChemStation was used to carry out each analysis. ICPMSDataCal (Liu et al., 2008) was used to perform offline selection and integration of the background and analytic signals as well as the time drift correction and quantitative calibration for the trace element analyses and U–Pb dating. Zircon 91500 was used as an external standard for the U–Pb dating and was analyzed twice for every five samples. The preferred U–Th–Pb isotope ratios used for the zircon 91500 were obtained from Wiedenbeck et al. (1995), and the uncertainty in these values was propagated to the sample results. Concordia diagrams were created and weighted mean calculations were performed using Isoplot/Ex (ver. 3) (Ludwig, 2003). In this study, the GJ-1 zircon yielded a mean age of 600 ± 3 (MSWD = 0.047, n = 12).

In situ Lu–Hf isotope analyses of the zircons were performed using a New Wave UP193 laser-ablation microprobe attached to a Neptune MC-ICP-MS at the State Key Laboratory for Mineral Deposits Research, Nanjing University. The instrumental conditions and data acquisition were similar to those described by Wu et al. (2006). A spot size of 60 μm and a repetition rate of 10 Hz were applied during all analyses. Helium was used as the carrier gas to transport the ablated samples from an LA cell to the ICP-MS torch.

To evaluate the accuracy of the LA results and to test the reliability of the correction protocols, we repeatedly analyzed two zircon standards: 91500 and Mud Tank (MT). Our analyses yielded a mean $^{176}Hf/^{177}Hf$ ratio of 0.282306 ± 0.000008 (2δ) for the zircon 91500 standard and 0.282490 ± 0.000004 (2δ) for the MT zircon standard. A decay constant of 1.865×10^{-11} yr^{-1} was adopted for ^{176}Lu (Scherer et al., 2001). The initial $^{176}Hf/^{177}Hf$ ratios, denoted as εHf(t), were calculated relative to the chondritic reservoir with the present-day $^{176}Hf/^{177}Hf$ ratio of 0.282772 and a $^{176}Lu/^{177}Hf$ ratio of 0.0332 (Blichert and Francis, 1997). The single-stage Hf model ages (T_{DM}) were calculated relative to the depleted mantle with a present-day $^{176}Hf/^{177}Hf$ ratio of 0.28325 and a $^{176}Lu/^{177}Hf$ ratio of 0.0384 (Vervoort and Blichert, 1999). The two-stage model ages (T_{DM2}) were calculated using an assumed $^{176}Lu/^{177}Hf$ ratio of 0.015 (Griffin et al.,

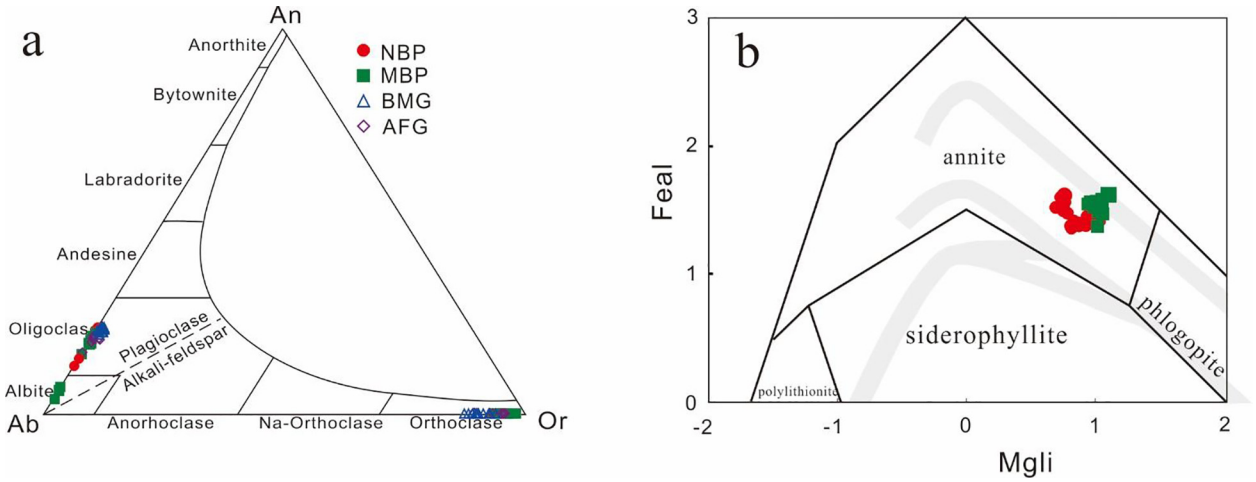

Fig. 5. Chemical characteristics of minerals from pegmatites. (a) Ternary classification diagram of feldspar (after Deer et al. 1979); (b) Trioctahedral Mg-Li classification diagram of mica (after Tischendorf et al., 2007).

2002).

5. Results

5.1. Mineral geochemistry

Electron microprobe analyses were performed to acquire compositional data for the feldspar (Supplementary Table 1) and biotite (Supplementary Table 2) grains from the NBP and MBP samples.

5.1.1. Feldspar

No systematic variations in the major elements among the feldspars from the NBP and MBP samples were obtained. The alkali-feldspars from the pegmatite samples have a high sodic content (Na_2O = 8.62%–11.16%) with high orthoclase (Or_{87}–Or_{98}) and low albite (Ab2–Ab13) concentrations. Plagioclases from the NBP and MBP samples are primarily represented by oligoclase (Fig. 5a).

5.1.2. Biotite

Biotite identified in the polished thin sections from the NBP and MBP samples were analyzed by EPMA. The biotite grains from the NBP samples are tiny, brown, and subhedral tabular (Fig. 3c). However, the biotite grains from the MBP samples are characterized by brown to dark brown, plumy aggregations (Fig. 3d). The variations in the cationic coefficients and the relevant parameters were calculated for biotite based on 22 oxygens. The Li_2O contents of the biotite are based on an empirical formula (Li_2O = [2.1/(0.356 + MgO)] − 0.088; Tischendorf Gerhard et al., 1999).

The $Fe^{2+}/(Fe^{2+} + Mg)$ values of the biotites in all the samples are relatively uniform, indicating that none of the biotites were modified by later fluids (Stone, 2000). Biotites in all the samples are enriched in iron with FeO_{total} values ranging from 18.96% to 25.86% and Mg# values ranging from 0.31 to 0.49. In the mica classification diagram (Tischendorf et al., 2007), all samples belong to Fe-rich annite (Fig. 5b). All the biotites were also enriched in TiO_2 (2.51%–4.11%), but were depleted in volatile components Cl (0.00%–0.03%) and F (0.00%–0.12%).

In the MBP biotites, the Al_2O_3 values range between 15.64% and 16.60%, aluminum saturation index ACNK values are from 1.46 to 1.63, MgO values are from 8.99% to 9.89%, and MnO values are from 0.32% to 0.42%. However, for the NBP biotites, the Al_2O_3 values are from 16.04% to 18.58%, aluminum saturation index ACNK values are from 1.48 to 1.83, MgO values are from 7.65% to 9.73%, and MnO values are from 0.12% to 0.44%. Relative to NBP, MBP biotite has higher MgO and MnO_2, lower Al_2O_3, and a lower aluminum saturation index, suggesting that MBPs were crystallized from more mafic magma, compared to the NBPs.

5.2. Whole-rock geochemistry

The bulk geochemistry data are listed in Supplementary Table 3.

Both the NBP and MBP samples are characterized by high SiO_2 (68.60–83.57%) and are subalkaline ($Na_2O + K_2O$ = 3.80%–11.34%) and peraluminous (ACNK = 1.02–1.16) (Fig. 6a, b). The Fe_2O_3, MgO, and K_2O contents vary significantly from 0.22% to 3.06%, 0.08% to 1.02%, and 0.87% to 8.53%, respectively. It is noteworthy that the bulk geochemistry of the pegmatites varies significantly owing to their coarse mineral grains and heterogeneous textures, especially for the MBP samples.

The chemical–mineralogical Q–P milicationic diagram (Debon and Le Fort, 1983) is usually used to evaluate mineralogical changes linked to the modifications in chemical composition of igneous rocks because it is sensitive to the proportion of quartz relative to alkali-feldspar and plagioclase. In the Q-P diagram (Fig. 6c), the pegmatites are scattered, indicating varying proportions of the main minerals. The plots of the MBP samples are similar to the uraniferous pegmatite in the Rössing deposit and the Trans-Hudson Orogen (Nex et al., 2001). When compared with NBP samples, the MBP samples are enriched in K-feldspar as evidenced by the Q-P diagram. This is consistent with the observations from hand specimens, in which many MBP samples are characterized by vast proportions of red microclines. From the peraluminous index A vs fractionation parameter B chemical–mineralogical diagram (Fig. 6d), some MBP samples are rich in iron oxides; this is consistent with the observation that many MBP samples are characterized by biotite clusters.

The total rare earth element (REE) contents of the NBP and MBP samples are relatively low but highly variable (ΣREE = 21.5–75.3 ppm for NBP and 22.6–35.5 ppm for MBP). Most of the NBP and MBP samples exhibit positive Eu anomalies (δEu = 0.7–11.6). The chondrite-normalized patterns of the NBP and MBP sample types are flat overall with a slight light REE (LREE) enrichment, and are similar to those of the host granites (Fig. 7a).

The trace element contents of the NBPs and MBPs vary significantly. In the primitive mantle-normalized spider diagram (Fig. 7b), both the NBP and MBP samples are rich in large-ion lithophile elements (e.g., Rb, U, Pb) but depleted in high-field-strength elements (e.g., P and Ti). The Th/U ratios of the NBP and MBP samples are relatively low (Th/U < 0.2; Fig. 8a). It is noteworthy that the Th/U ratios decrease from the granites to the pegmatites owing to a substantial increase in U contents and constant Th contents, as is seen in other pegmatite-type

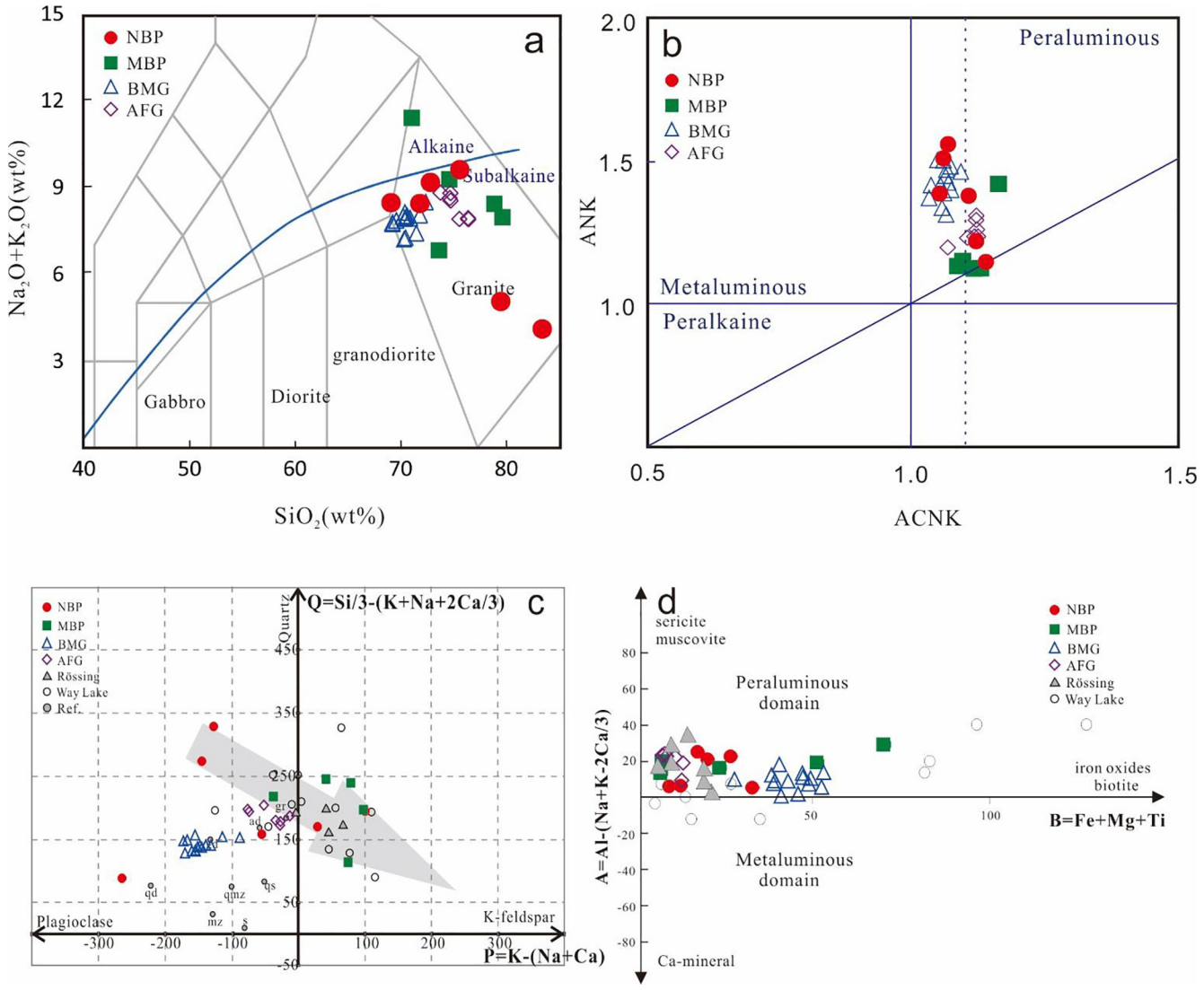

Fig. 6. Geochemical classification diagrams for the pegmatites. (a) (K_2O + Na_2O) vs. SiO2 (TAS) diagram (after Middlemost, 1994), (b) A/NK vs. A/CNK diagram (after Maniar and Piccoli, 1989), (c) Q-P classification diagram (after Debon and Le Fort, 1983) and (d) A-B classification diagram (after Debon and Le Fort, 1983). Data sources for the BMG and AFG from Huichizi complex (Chen et al., 2018), Rossing (Cuney and Kyser, 2015), Way lake (Mercadier et al., 2013) and Ref. (average composition of main plutonic rock type, from Debon and Le Fort, 1983). Abbreviations: ad = adamellite, bt = biotite, gd = granodiorite, gr = granite, ms = muscovite, mz = monzonite, qd = quartz diorite, qmz = quartz monzonite, qs = syenite quartz, s = syenite.

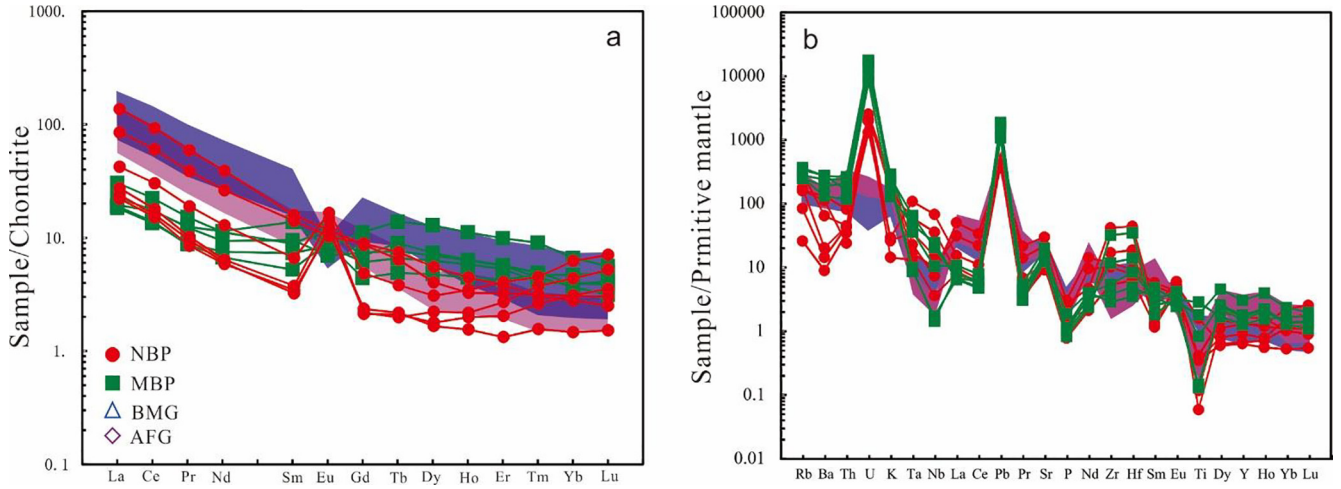

Fig. 7. (a) Chondrite-normalized REE patterns and (b) primitive mantle (PM) normalized trace element diagrams for NBP and MBP. The values of chondrite and PM are from Sun and McDonough (1989).

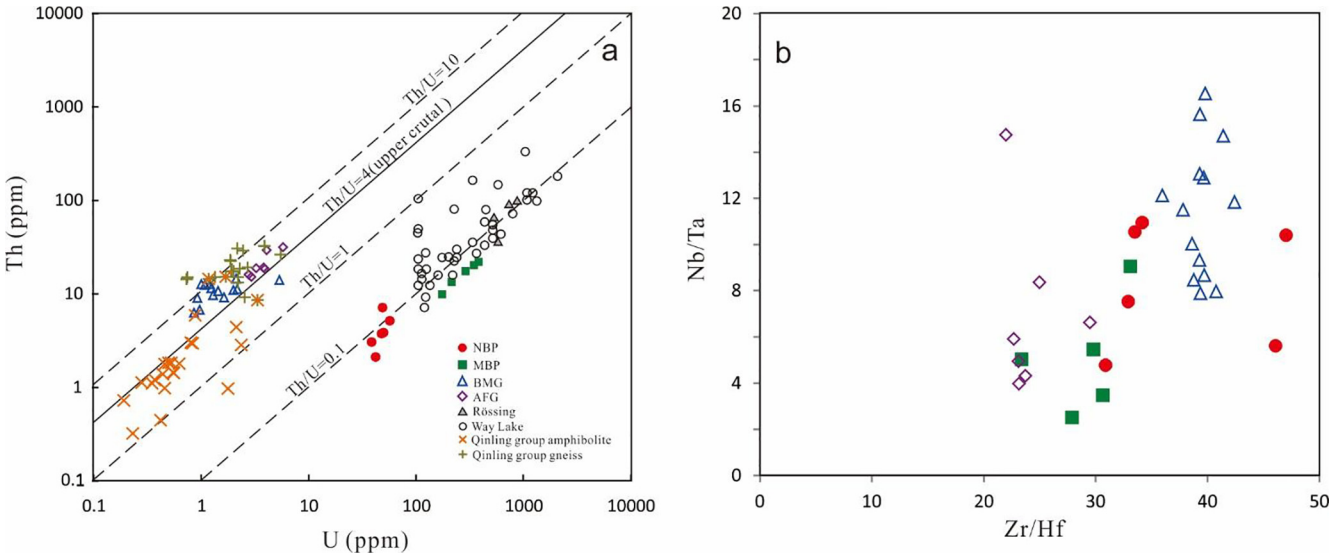

Fig. 8. (a) U vs. Th and (b) Nb/Ta vs. Zr/Hf diagrams of pegmatites. Data sources for the BMG and AFG from Huichizi complex (Chen et al., 2018), Rossing (Cuney and Kyser, 2015), Way lake (Mercadier et al., 2013) and Qinling group gneiss (Yang et al., 2010; Shi et al., 2013; Liu, 2014).

uranium deposits (McKeough et al., 2013; Cuney and Kyser, 2015).

5.3. Zircon U–Pb dating

Most of the zircon fractions are obscure or murky in the cathodoluminescence (CL) images; however, some show relatively slight oscillatory zonation (Fig. 4d). Ablation points were selected on the oscillatory zone, excluding inclusions, fractures, porosities, and highly metamict areas when possible (Fig. 4d).

The entire U–Pb zircon analytical dataset is presented in Supplementary Table 4 and plotted in the Concordia diagrams in Fig. 9a and b. Ages of less than 1000 Ma are ^{204}-corrected $^{206}Pb/^{238}U$, whereas ages greater than 1000 Ma are ^{204}-corrected $^{207}Pb/^{206}Pb$.

A total of 37 analyses from the NBP and MBP samples were conducted for the zircon fractions. The zircon fractions from the MBP samples yielded $^{206}Pb/^{238}U$ ages ranging from 411 to 427 Ma (except for two zircon fractions with distinct inherited cores) with a weighted mean of 419 ± 2 Ma (MSWD = 1.5). For the NBP samples, the $^{206}Pb/^{238}U$ ages ranged from 413 to 425 Ma (except for four zircon fractions with distinct inherited cores) with a weighted mean of 419 ± 2 Ma (MSWD = 0.7).

Six inherited zircon cores from the pegmatites were analyzed. Two analyses on NBP zircon fractions yielded a $^{207}Pb/^{206}Pb$ age of 1461 Ma and a $^{206}Pb/^{208}Pb$ age of 930 Ma, and four analyses on MBP zircon grains yielded $^{207}Pb/^{206}Pb$ ages of 1591 Ma and 1751 Ma, and $^{206}Pb/^{208}Pb$ ages of 552 Ma and 565 Ma.

5.4. Lu–Hf isotope composition

The entire Lu–Hf isotope analytical dataset is presented in Supplementary Table 5. The εHf(t) values were calculated using the weighted mean $^{206}Pb/^{238}U$ age, as determined by the zircon U–Pb method. The $^{176}Lu/^{177}Hf$ ratios are less than 0.002 for the tested zircons, meaning that ^{176}Hf was rarely generated by ^{176}Lu decay and that the test $^{176}Lu/^{177}Hf$ ratio can represent the Hf isotopic composition of the source (Amelin et al., 1999; Wu et al., 2006). The $f_{Lu/Hf}$ of the zircons is between −0.98 and −0.96, lower than those of a mafic lower crust (−0.34; Amelin et al., 1999) and silica-rich crust (−0.72; Vervoort et al., 1996). Therefore, the Hf isotopic model age (T_{DM2}) of the zircons may represent the time that the source rock separated from

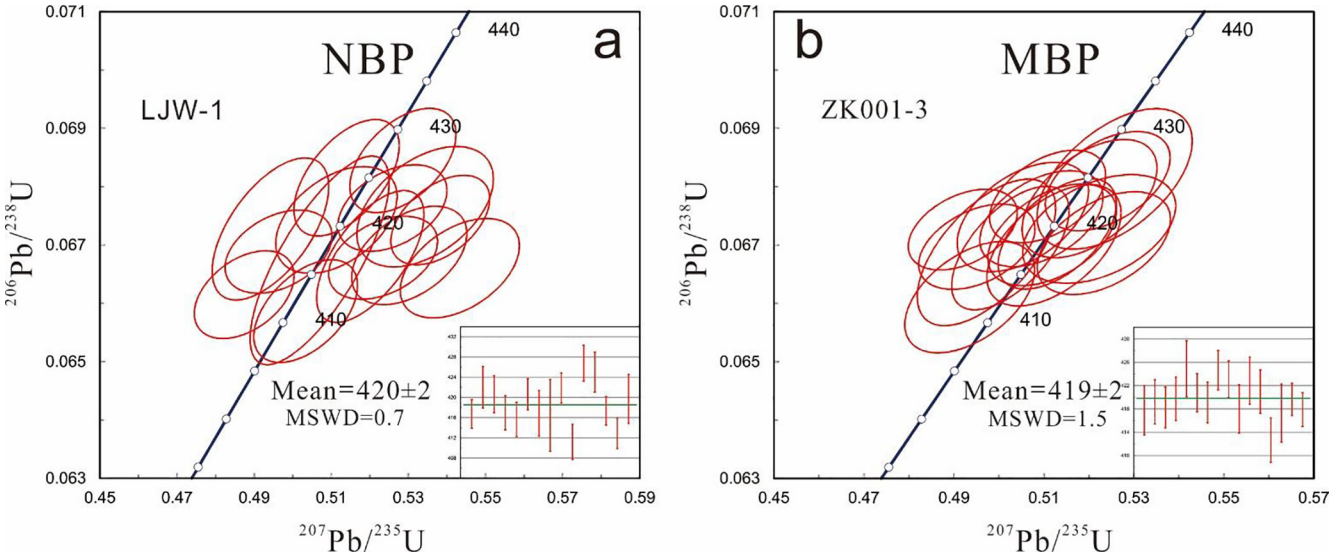

Fig. 9. Zircon LA-ICP-MS concordia diagrams for NBP (a) and MBP (b). The weighted mean age and MSWD are shown in each figure.

the mantle.

A total of 34 zircons from the NBP and MBP samples were analyzed. Zircons from the NBP sample were observed to have a narrow range of initial $^{176}Hf/^{177}Hf$ from 0.282390 to 0.282589, with εHf values ranging from −4.5 to +2.6. The MBP sample yielded a similar range of initial $^{176}Hf/^{177}Hf$ ratios from 0.282378 to 0.282598, with εHf values ranging from −5.1 to +2.8. Both the samples showed Paleoproterozoic to Mesoproterozoic two-stage Hf model ages from 1723 to 1227 Ma.

6. Discussion

6.1. Time of mineralization

Previous studies have shown that zircons can be of magmatic or hydrothermal origin, and that the internal structure and zoning, morphology, and trace element geochemistry of zircons can aid in distinguishing these origins (e.g., Pettke et al., 2005; Pelleter et al., 2007; Schaltegger et al., 2007; Fu et al., 2009). All the analyzed zircon fractions exhibit Th/U ratios below 0.1, which is notably lower than that for a typical magmatic origin (Th/U > 0.2), indicating a hydrothermal origin (Hoskin and Black, 2000; Belousova et al., 2002). However, we conclude that the zircon fractions show some characteristics of magmatic zircon, and may have crystallized from the volatile-rich pegmatite magma. The reasoning behind this inference is as follows: (1) the zircon fractions in the pegmatites are usually interstitial to high temperature uraninite (with high ThO_2 content > 3% and heavy REE (HREE) rich, unpublished data), and is enclosed in quartz or plagioclase (Fig. 4a); (2) the zircon fractions are prismatic and colorless (Fig. 4b), and backscattered electron (BSE) images of zircons are relatively clean without obvious zoning or the occurrence of uranium or lead rich phosphate, indicating that any hydrothermal effect on zircon is negligible (Fig. 4c). (3) CL imaging of analyzed zircon shows relatively slight oscillatory zonation (Fig. 4d), indicating that the metamict effect did not damage the structure of the zircon. Therefore, the weighted mean $^{206}Pb/^{238}U$ age of the zircons is interpreted as the crystallization age of the pegmatite. The crystallization age of the zircons is interpreted as the mineralization age owing to the intergrowth relationship with uraninite (Fig. 4a, b).

Two samples from the NBP and MBP yielded the same age within the uncertainty error (420 ± 2 Ma for the MBP sample and 419 ± 2 Ma for the NBP sample). Therefore, it is reasonable to infer that the pegmatite dikes intruded at 422–417 Ma.

Moreover, the four inherited zircon cores with high Th/U ratios (> 0.1) yielded $^{207}Pb/^{206}Pb$ ages of 1751, 1591 and 1461 Ma and a $^{206}Pb/^{208}Pb$ age of 930 Ma. These ages of the inherited cores are consistent with the depositional time-interval of the Qinling Group, indicating that the Qinling Group was involved in the formation of the pegmatites. The two inherited zircon cores with low Th/U ratios (< 0.02) yielded $^{206}Pb/^{208}Pb$ ages of 552 and 565 Ma, and may indicate thermal events, as no magmatic activity is known to have occurred in this area during that time.

In conclusion, the zircon LA-ICPMS U–Pb dating indicates that the formation of the pegmatite as well as uranium mineralization occurred during the Caledonian (422–417 Ma).

6.2. Derivation of pegmatites

Many studies have focused on the derivation of the biotite pegmatites in the Guangshigou uranium deposits (Wan et al., 1992; Zeng and Jin, 1994; Feng et al., 1996; Sha et al., 2011; Yuan et al., 2018). Some researchers believe that the biotite pegmatites are derived from the crystallization of the Huichizi pluton, based on their close spatial relationship and similar bulk chemistry and mineralogy (Wan et al., 1992; Sha et al., 2011). Other researchers argue that the biotite pegmatites may have been derived from the partial melting of mantle material and the Qinling Group based on the Sr–Nd isotopic characteristics of the Huichizi granites (Feng et al., 1996). However, both statements lack systemic chronological and isotopic evidence.

Our zircon U–Pb dating of pegmatite indicates that the biotite pegmatite intruded at 422–417 Ma, which is similar to the emplacement age of the AFGs (424 Ma; Chen et al., 2018). Therefore, the fractional crystallization model seems more appropriate, considering their close spatial and temporal relationship. However, the mineralogy and geochemistry of the biotite pegmatites and AFGs do not support the crystallization model. The reasons are as followings.

1. The biotite pegmatites contain a relatively higher biotite proportion compared with AFGs; the latter have a small quantities of biotite (< 5%), indicating that the melt of the pegmatites had more mafic characteristics that should have been reduced if fractionation were important.
2. It is difficult to use the major and trace elements to demonstrate the changes from granites to pegmatites owing to the varying proportions of the major minerals. However, “geochemical twins,” which are controlled by minor minerals, can be used to demonstrate crystallization. Zr–Hf and Nb–Ta, which are typically incompatible elements, are considered to be geochemical twins owing to their identical charge and similar ionic radii. In felsic igneous systems, these elements may enter accessory minerals (such as zircon and monazite) during fractional crystallization, which can cause fractionations of Zr from Hf and Nb from Ta. Therefore, a continual decrease in the Zr/Hf and Nb/Ta ratios is expected to occur with fractional crystallization in peraluminous magma (Stepanov et al., 2014). The Nb/Ta and Zr/Hf ratios are similar for the AFGs and pegmatites, without a clear decreasing trend (Fig. 8b). This indicates that the relationship between the AFGs and the pegmatites is not determined by fractional crystallization.
3. The Hf isotope ratios of the zircons from the biotite pegmatites yield a range of initial $^{176}Hf/^{177}Hf$ ratios from 0.282378 to 0.282598, with εHf values ranging from −5.1 to +2.8, which is much lower than those of the granites (εHf(t) = +0.6–+8.5; Chen et al., 2018). This indicates that larger amounts of ancient crustal materials were involved in the origin of the pegmatites compared with that of the host granites. The positive to negative εHf(t) values are similar to those of the Qinling Group basement-derived rocks in NQB (Shi et al., 2013; Diwu et al., 2014). In addition, the plots of the pegmatites fall on the evolutionary trends of the Qinling Group in the εHf(t)–t diagram (Fig. 10). Thus, the pegmatites likely were derived

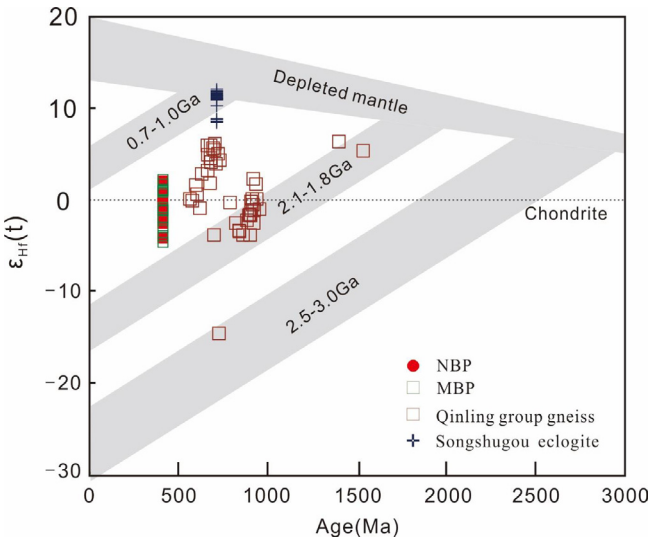

Fig. 10. $^{206}Pb/^{238}U$ ages vs $\varepsilon_{Hf}(t)$ diagram of zircons from the pegmatites. Data sources for the Qinling group gneiss (Yan et al., 2009; Liu, 2014), and Songshugou eclogite (Qian et al., 2013; Wang et al., 2013a).

from partial melting of the Qinling Group rocks. However, small amounts of juvenile lower crustal material may have been involved in the derivation of the biotite pegmatite, considering the high variation in the εHf(t) of their zircons and their close spatial and temporal relationships with the Huichizi granites, the source materials of which involved significant amounts of juvenile lower crust (Qin et al., 2015; Chen et al., 2018).

Therefore, the pegmatites likely were derived from the anatexis of the Qinling Group rocks but with an input of small amount of juvenile lower crustal materials.

6.3. Mineralization of uranium

Uranium in silicate magmas is prevented from being incorporation into the structures of the main rock-forming silicates owing to its large ionic radius and high valence. As a result, during partial melting and crystal fractionation, U is preferentially fractionated into silicate melts (Cuney and Kyser, 2015).

Theoretically, there are two ways in which a granitic pluton with abundant uranium can be produced. One is the extreme fractional crystallization of highly fractionated silicate magma. However, for the particular Guangshigou deposit, this mechanism can be excluded owing to the derivation of the pegmatites from partial melting as well as the low depolymerization (K + Na/Al) of the granitic melt, which is significant to the solution of the uranium content (Peiffert et al., 1996). Another way in which a silicate melt can become uranium-rich is by the low-degree partial melting of the source rocks (Robb, 2004; Mercadier et al., 2013). Robb (2004) demonstrated that if the degree of partial melting is very low (i.e., < 5%), the concentrations of U in granitic melts can reach 300 ppm. Using model calculations, Kukkonen and Lauri (2009) confirmed that uranium can be enriched by tens of times that of the protolith via low degrees of partial melting. Therefore, partial melting with low melt volumes can result in high concentrations of U content in the melt even with even a normal U content in the source material.

Meanwhile, Th exhibits similar geochemical behavior to that of U owing to its similar radius and valence in the melt and granite. Theoretically, Th should be enriched to the same extent as U under low partial melting, which interferes with the formation of uraninite owing to the priority of the thorite, uranothorite, or monazite, and the Th/U ratio should be stable from the source to the melt. However, the Th/U ratios of the biotite pegmatites are notably lower than those in the granite (Fig. 8a), the Qinling Group, and the upper continental crust, indicating preferential U enrichment during partial melting. Two alternations can aid in explaining this: a) magma is derived from U-rich and Th-depleted source rocks, something that has never been reported in the NQB; b) the presence of a Th-rich resident minerals in the source during partial melting.

Monazite and/or allanite are the primary repositories of U and Th in most metasedimentary rocks and are the main contributors of these elements to anatectic melts (Bea, 1996; Hermann, 2002; Janots et al., 2008; Skora and Blundy 2010). Thus, the behavior of monazite/allanite could be responsible for the contents of these elements in the melt during partial melting. Experimental studies show that the monazite/melt partition coefficients for U are much lower than those for Th and the LREEs (Skora and Blundy, 2010; Stepanov et al., 2012; Xing et al., 2013). Therefore, anatectic melts buffered by monazite/allanite should be enriched in U relative to Th, which can be confirmed from the U/Th ratio of the pegmatites and the Qinling Group rocks (Fig. 8a). This is in agreement with the presence of peritectic melt inclusions with high U contents and low Th/U ratios (Acosta-Vigil et al., 2010), as well as observations of monazites with Th-rich cores in granulites, which are regarded as residual grains from peak melting conditions (Zhu and O'Nions, 1999). Although the U contents of the Qinling group gneisses are quite low (mostly < 2 ppm), a few studies have reported that some gneisses in Qinling group are rich in uranium (5–20 ppm, Feng et al., 1996; No. 224 group of China National Nuclear Corporation, 2008; Yang et al., 2010). Therefore, low-degree partial melting of the Qinling Group with monazite/allanite residuals should be the main mechanism for the derivation of the uranium-rich pegmatites. A similar mechanism could be responsible for the high U and low Th/U ratios of arc melts in subduction zones (Plank, 2005; Hermann and Rubatto, 2009; Skora and Blundy, 2010).

The NBPs are characterized by high uranium contents (> 40 ppm) and the MBP uranium content is extremely high (> 150 ppm). Field geological observation and microscopic identification show that both NBPs and MBPs have nearly identical chemical and mineral compositions but different textures (Fig. 3c, d). Most of the MBPs exhibit more heterogeneous textures and are characterized by plumy biotite. Uranium-mineralization pegmatites characterized by plumy biotite have been reported by many researchers (Lentz, 1996; McKeough et al., 2013). They are always developed at the edges of pegmatite and sedimentary wall rocks. Previous studies indicate that the plumy aggregation texture can be regarded as a sign of assimilation (Beard et al., 2005; Clarke et al., 2007). Meanwhile, the differentiation in the chemical characteristics of the biotite between NBPs and MBPs can be the result of assimilation. Experimental studies have shown that when the melt temperature is low (< 700 °C), assimilation primarily proceeds via mineral selective decomposition and element exchange between the host and wall rock, resulting in a newborn biotite enriched in Mg, Fe, Mn, and Ti, but depleted in Al (Beard et al., 2005; Erdmann et al., 2007). The EPMA data show that, relative to NBP, the MBP biotite has higher MgO, FeOt, TiO_2, and MnO_2 contents, and lower Al_2O_3 content, which confirms that assimilation occurred between a pegmatitic melt and the sedimentary wall rock (the Qinling Group in this case). Assimilation may cause massive crystallization of plumy biotites, significantly decreasing the content of F in the melt, which is the most important carrier of uranium. Conversely, large quantities of Th, U, and REE accessory minerals can crystallize near the assimilation zone (Lentz, 1996). The phenomenon of zircon grains coexisting with uraninite near the plumy biotite confirms this explanation, as does the trace elemental data for the zoned zircon from the hybrid part of the pegmatite (Yuan et al., 2018).

On the other hand, as mentioned earlier, a few MBPs are characterized by cores of smoky quartz and pink oligoclase. Previous studies have shown that high volumes of quartz and pink oligoclase in biotite pegmatites are always developed at the inner center as a core, which can be regarded as the most evolved part of the biotite pegmatites. The core represents the evolved part of the pegmatite via crystallization fractionation (London, 2014). Uranium is an incompatible element in peraluminous melts, and tends to be enriched in the evolved melt. Th and REE-rich accessory minerals, such as monazite and zircon, crystallize at an early stage owing to their low solubility in peraluminous melts, leading to significant depletion in Zr, Th, and REEs. After the crystallization fractionation of these minerals, uraninite can crystallize when the temperature decreases and uranium saturation is reached. This is why uraninite is always found in highly evolved peraluminous leucogranites (Chen et al., 2012; Hu et al., 2012; Ballouard et al., 2017). Therefore, MBP, which is characterized by smoky quartz and pink feldspar, may represent the evolved part of the uraniferous biotite pegmatite.

Therefore, low-degree partial melting of the Qinling Group with monazite/allanite as residuals may be the main mechanism for the derivation of the uranium-rich pegmatites. The assimilation between the biotite pegmatite dikes and the wall rock may be the most significant mechanisms for the large-scale formation of uranium mineralization in the biotite pegmatite, and also the fractional crystallization of the pegmatitic magma may be another mechanism for the uranium mineralization

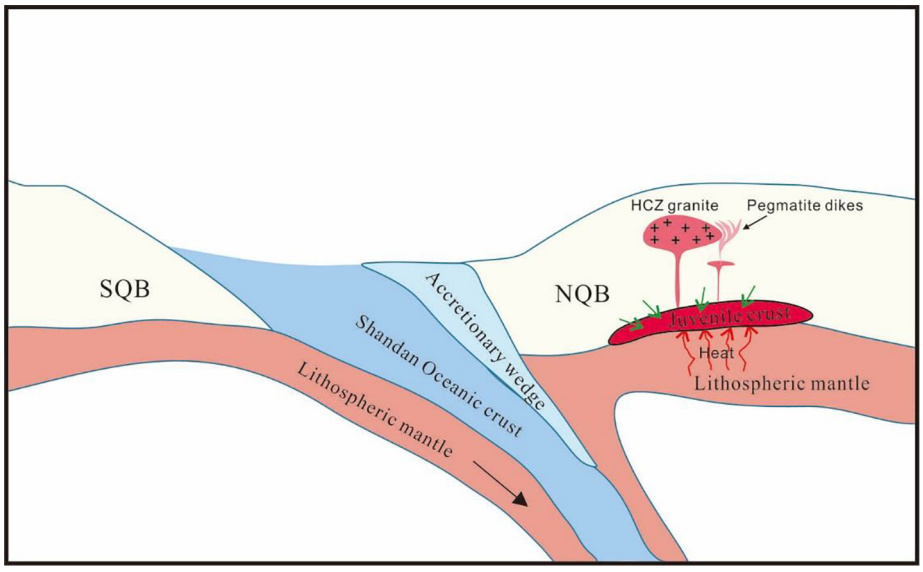

Fig. 11. Schematic diagram of the formation of the pegmatites. The exhumation of the subducted Shangdan oceanic crust beneath the NQB unit resulted in the amphibolite facies metamorphism and the anatexis of the lower crust at ~420 Ma. The Qinling Group rocks were heated to low degree of partial melting owing to the present of fluids from the dehydration of the hydrous minerals. The melt which was characterized by enrichment in uranium and volatile, would have been channeled along vertical structures in the upper crust and then crystallized as the pegmatite dikes around the Huichizi granites. Abbreviations are: SQB: South Qinling Block; NQB: North Qinling Block; HCZ granite: Huichizi granite.

6.4. Tectonic implications

Multiphase metamorphic and magmatic events were widespread in the NQB and were accompanied by the formation of numerous igneous and metamorphic rocks, making the NQB a classic case study of the evolution of a structure belt. Highly precise ages of high–ultrahigh pressure Paleozoic metamorphic rocks have been acquired in recent years (Liu et al., 2009, 2013; Chen et al., 2015). It is generally known that the NQB underwent deep subduction and exhumation of the continental crust in the Paleozoic via three episodes of magmatic and metamorphic events (~500, ~450, and ~420 Ma; Wang et al., 2009; Liu et al., 2013; Wu and Zheng, 2013; Dong et al., 2016; Yu et al., 2016).

Zircon U–Pb dating indicates that the uranium-rich pegmatite dikes were intruded ~420 Ma. Previous studies have shown that only a few granites and migmatites are reported at ~420 Ma in the NQB, demonstrating that the magmatic activity was relatively weak and that the collisional orogeny was drawing to a close. However, amphibolite facies metamorphism occurred at 420 Ma in the NQB, caused by the exhumation of a subducted slab (Cheng et al., 2011; Liao et al., 2016; Ratschbacher et al., 2003). The exhumation of a subducted slab can cause the decomposition and hydroxyl exsolution of hydrous minerals owing to a decrease in the pressure and the production of fluids (Zheng, 2011). These fluids can then reduce the solidus of the protolith. With decompression melting, partial melting was limited to a low degree and a small scale owing to the low temperature and pressure, which can be confirmed by the plentiful inherited cores in the zircons and the small scale of the pegmatite dikes. The low degree of partial melting with monazite as the residual mineral produced a granitic melt with significant uranium enrichment. The melts would then have been collected and channeled along vertical structures in the upper crust and then crystalized as the uranium-rich pegmatite dikes (Fig. 11). Therefore, amphibolite (or granulite) facies metamorphism, caused by the exhumation of a subducted slab in the NQB, may have been an important factor in the genesis of the uranium-rich pegmatitic magma and the formation of the Guangshigou pegmatite-type uranium deposit. Similar mechanisms may have arisen with the uraniferous pegmatites of the Wollaston Domain and Grenville Province in Canada and the Rössing district in Namibia, which is thought to be related to upper-amphibolite- to granulite-facies metamorphism (Ward et al., 2008; McKeough et al., 2013).

7. Conclusions

Following major conclusions can be drawn from this study:

1. The zircon LA-ICPMS U–Pb dating of the uraniferous pegmatite dikes indicates that the dikes intruded in the Caledonian (422–417 Ma).
2. The uranium-rich biotite pegmatite dikes were derived from low-degree partial melting of the Qinling Group with monazite/allanite as the residual minerals, but small amounts of juvenile materials were also present.
3. The assimilation between the pegmatite dikes and the wall rock may be the primary mechanism that resulted in uranium mineralization in the biotite pegmatite, while the fractional crystallization of the melt was the secondary mechanism.
4. The exhumation of a subducted slab in the NQB, which led to amphibolite (or granulite) facies metamorphism, may have been an important factor for the genesis of the uranium-rich pegmatitic magma and the formation of the Guangshigou pegmatite-type uranium deposit.

Acknowledgments

The authors are grateful to Dr. Hu Zhaochu from China University of Geosciences and Dr. Yang Tao from Nanjing University for their great help with expert isotopic analysis support. We appreciate the guest editor and two anonymous reviewers, who improved the paper greatly.

Funding

This research was financially supported by the Strategic Priority Research Program (B) of Chinese Academy of Sciences (Grant No. XDB18030200), and National Natural Sciences Foundations of China (41473049, 41103027).

Appendix A. Supplementary data

Supplementary data to this article can be found online at https://doi.org/10.1016/j.oregeorev.2019.103165.

References

Acosta-Vigil, A., Buick, I., Hermann, J., Cesare, B., Rubatto, D., London, D., Morgan George, B., 2010. Mechanisms of crustal anatexis: a geochemical study of partially

melted metapelitic enclaves and host dacite, SE Spain. J. Petrol. 51, 782–785.
Amelin, Y., Lee, D.C., Halliday, A.N., Pidgeon, R.T., 1999. Nature of the Earth's earliest crust from hafnium isotopes in single detrital zircons. Nature 399, 252.
Austman, C.L., Ansdell, K.M., Annesley, I.R., 2010. Petrography and geochemistry of granitic pegmatite-and leucogranite-hosted uranium & thorium mineralization: Fraser Lakes Zone B, northern Saskatchewan, Canada.
Ballouard, C., Poujol, M., Boulvais, P., Mercadier, J., Tartèse, R., Venneman, T., Deloule, E., Jolivet, M., Kéré, I., Cathelineau, M., Cuney, M., 2017. Magmatic and hydrothermal behavior of uranium in syntectonic leucogranites: the uranium mineralization associated with the Hercynian Guérande granite (Armorican Massif, France). Ore Geol. Rev. 80, 309–331. https://doi.org/10.1016/j.oregeorev.2016.06.034.
Basson, I.J., Greenway, G., 2004. The Rössing Uranium Deposit: a product of late-kinematic localization of uraniferous granites in the Central Zone of the Damara Orogen, Namibia. J. African Earth Sci. 38, 413–435. https://doi.org/10.1016/j.jafrearsci.2004.04.004.
Bea, F., 1996. Residence of REE, Y, Th and U in Granites and Crustal Protoliths; Implications for the Chemistry of Crustal Melts. J. Petrol. 37, 521–552.
Beard, J.S., Ragland, P.C., Crawford, M.L., 2005. Reactive bulk assimilation: a model for crust-mantle mixing in silicic magmas. Geology 33, 681–684.
Belousova, E., Griffin, W., O'Reilly, S.Y., Fisher, N., 2002. Igneous zircon: trace element composition as an indicator of source rock type. Contrib. Mineral. Petrol. 143, 602–622. https://doi.org/10.1007/s00410-002-0364-7.
Blichert-Toft, J., Albarède, F., 1997. The Lu-Hf isotope geochemistry of chondrites and the evolution of the mantle-crust system. Earth Planet. Sci. Lett. 148, 243–258. https://doi.org/10.1016/S0012-821X(97)00040-X.
Chen, D.L., Ren, Y.F., Gong, X.K., Liu, L., Gao, S., 2015. Identification and its geological significance of eclogite in Songshugou, the North Qinling. Acta Petrol. Sin. 31, 1841–1854 (in Chinese with English abstract).
Chen, Y.W., Bi, X.W., Hu, R.Z., Dong, S.H., 2012. Element geochemistry, mineralogy, geochronology and zircon Hf isotope of the Luxi and Xiazhuang granites in Guangdong province, China: implications for U mineralization. Lithos 150, 119–134. https://doi.org/10.1016/j.lithos.2012.06.025.
Chen, Y.W., Bi, X.W., Hu, R.Z., Dong, S.H., Cheng, D.J., Feng, Z.S., 2013. Mineral chemistry of biotite and its implications for uranium mineralization in guangshigou pegmatite-type uranium deposit, south shaanxi province. J. Mineral. Petrol. 33 (4), 17–28 (in Chinese with English abstract).
Chen, Y.W., Hu, R.Z., Bi, X.W., Dong, S.H., Zhou, T., 2018. Zircon U-Pb Ages and Sr-Nd-Hf Isotopic Characteristics of the Huichizi Granitic Complex in the North Qinling Orogenic Belt and Their Geological Significance. J. Earth Sci. 29 (3), 492–507.
Cheng, H., Zhang, C., Vervoort, J.D., Li, X., Li, Q., Zheng, S., Cao, D., 2011. Geochronology of the transition of eclogite to amphibolite facies metamorphism in the North Qinling orogen of central China. Lithos 125, 969–983. https://doi.org/10.1016/j.lithos.2011.05.010.
Clarke, D.B., 2007. Assimilation of xenocrysts in granitic magmas: principles, processes, proxies, and problems. Can. Mineral. 45, 5–30.
Cuney, M., 2011. Uranium and thorium: The extreme diversity of the resources of the world's energy minerals. In: Sinding-Larsen, R., Wellmer, F.-.W. (Eds.), Non-Renewable Resource Issues: Geoscientific and Societal Challenges, International Year of Planet Earth. Springer, New York, pp. 91–129.
Cuney, M., 2012. Uranium and Thorium: The Extreme Diversity of the Resources of the World's Energy Minerals. Springer, Netherlands.
Cuney, M., Kyser, T.K., 2015. The Geology and Geochemistry of Uranium and Thorium Deposits. Mineralogical Association of Canada.
Debon, F., Le Fort, P., 1983. A chemical–mineralogical classification of common plutonic rocks and associations. Earth Environ. Sci. Trans. R. Soc. of Edinburgh 73 (3), 135–149.
Deer, W.A., Howie, R.A., Zussman, J., 1979. An Introduction to the Rock Forming Minerals. Longman, London, UK.
Diwu, C.R., Sun, Y., Zhao, Y., Liu, B., Lai, S., 2014. Geochronological, geochemical, and Nd-Hf isotopic studies of the Qinling Complex, central China: implications for the evolutionary history of the North Qinling Orogenic Belt. Geosci. Front. 5, 499–513. https://doi.org/10.1016/j.gsf.2014.04.001.
Dong, Y.P., Santosh, M., 2016. Tectonic architecture and multiple orogeny of the Qinling Orogenic Belt. Central China. Gondwana Res. 29, 1–40. https://doi.org/10.1016/j.gr.2015.06.009.
Dong, Y.P., Zhang, G., Hauzenberger, C., Neubauer, F., Yang, Z., Liu, X., 2011. Palaeozoic tectonics and evolutionary history of the Qinling orogen: Evidence from geochemistry and geochronology of ophiolite and related volcanic rocks. Lithos 122, 39–56.
Erdmann, S., London, D., Morgan, G.B., Clarke, D.B., 2007. The contamination of granitic magma by metasedimentary country-rock material: an experimental study. Can. Mineral. 45 (1), 43–61.
Fayek M., 2013.Uranium ore deposits: a review. Uranium: cradle to grave, 43:121–147.
Feng, M.Y., Rong, J.S., Sun, Z.F., 1996. the Pegmatite-Type Uranium Deposit in North Qinling. Atomic Energy Press, Beijing (in Chinese).
Feng, Z.S., Chen, J.L., Cheng, D.J., Zhou, L., Zhang, X.T., 2015. Characteristics of host rock and uranium mineralization in Guangshigou uranium deposit. World Nucl. Geosci. 32 (4), 200–207 (in Chinese with English abstract).
Fu, B., Mernagh, T.P., Kita, N.T., Kemp, A.I., Valley, J.W., 2009. Distinguishing magmatic zircon from hydrothermal zircon: a case study from the Gidginbung high-sulphidation Au–Ag–(Cu) deposit, SE Australia. Chem. Geol. 259 (3–4), 131–142.
Griffin, W.L., Wang, X., Jackson, S.E., Pearson, N.J., O'Reilly, S.Y., Xu, X., Zhou, X., 2002. Zircon chemistry and magma mixing, SE China: in-situ analysis of Hf isotopes, Tonglu and Pingtan igneous complexes. Lithos 61, 237–269. https://doi.org/10.1016/S0024-4937(02)00082-8.
Hermann, J., 2002. Allanite: thorium and light rare earth element carrier in subducted crust. Chem. Geol. 192 (3–4), 289–306.
Hermann, J., Rubatto, D., 2009. Accessory phase control on the trace element signature of sediment melts in subduction zones. Chem. Geol. 265, 512–526. https://doi.org/10.1016/j.chemgeo.2009.05.018.
He, H.J., Zhao, J.F., Zang, Y.S., Qian, B., Wang, D.S., Hu, X.J., Yang, L.Q., 2018. Geochemical characteristics and genetic analysis of granite pegmatite dikes in Guangshigou area, Qingling. Uranium Geol. 34 (2), 73–80 (in Chinese with English abstract).
Hoskin, P.W.O., Black, L.P., 2000. Metamorphic zircon formation by solid-state recrystallization of protolith igneous zircon. J. Metamorph. Geol. 18, 423–439. https://doi.org/10.1046/j.1525-1314.2000.00266.x.
Hu, H., Wang, R., Chen, W.F., Ding, H., Chen, P.R., Ling, H.F., 2012. Study on uranium resource minerals of Douzhashan uranium-bearing granite, Northeastern Guangxi. Geol. Rev. 58 (6), 1056–1068.
International Atomic Energy Agency, 2018. Geological Classification of Uranium Deposits and Description of Selected Examples, IAEA TECDOC Series. IAEA, Vienna.
Janots, E., Engi, M., Berger, A., Allaz, J., Schwarz, J.O., Spandler, C., 2008. Prograde metamorphic sequence of REE minerals in pelitic rocks of the Central Alps: implications for allanite–monazite–xenotime phase relations from 250 to 610 C. J. Metamorph. Geol. 26 (5), 509–526.
Kinnaird, J.A., Nex, P.A.M., 2007. A review of geological controls on uranium mineralisation in sheeted leucogranites within the Damara Orogen, Namibia. Appl. Earth Sci. 116, 68–85. https://doi.org/10.1179/174327507X167091.
Kukkonen, I.T., Lauri, L.S., 2009. Modelling the thermal evolution of a collisional Precambrian orogen: high heat production migmatitic granites of southern Finland. Precambr. Res. 168, 233–246. https://doi.org/10.1016/j.precamres.2008.10.004.
Lentz, D., 1996. U, Mo, and REE mineralization in late-tectonic granitic pegmatites, southwestern Grenville Province, Canada. Ore Geol. Rev. 11, 197–227. https://doi.org/10.1016/0169-1368(95)00034-8.
Liao, X., Liu, L., Wang, Y., Cao, Y., Chen, D., Dong, Y., 2016. Multi-stage metamorphic evolution of retrograde eclogite with a granulite-facies overprint in the Zhaigen area of the North Qinling Belt, China. Gondwana Res. 30, 79–96. https://doi.org/10.1016/j.gr.2015.09.012.
Liu, B.X., 2014. Magmatism and crustal evolution inthe eastern North Qinling Terrain. University of Science and Technology of China. Anhui A dissertation for doctor's degree (in Chinese with English abstract).
Liu, J., Sun, Y., Tong, L., Sun, W., 2009. Emplacement age of the Songshugou ultramafic massif in the Qinling orogenic belt, and geologic implications. Int. Geol. Rev. 51, 58–76. https://doi.org/10.1080/00206810802650576.
Liu, L., Liao, X.Y., Zhang, C.L., Chen, D.L., Gong, X.K., Kang, L., 2013. Multi-matemorphic timings of HP-UHP rocks in the North Qinling and their geological implications. Acta Petrol. Sin. 29, 1634–1656.
Liu, Y., Hu, Z., Gao, S., Günther, D., Xu, J., Gao, C., Chen, H., 2008. In situ analysis of major and trace elements of anhydrous minerals by LA-ICP-MS without applying an internal standard. Chem. Geol. 257, 34–43. https://doi.org/10.1016/j.chemgeo.2008.08.004.
London, D., 2014. A petrologic assessment of internal zonation in granitic pegmatites. Lithos 184–187, 74–104. https://doi.org/10.1016/j.lithos.2013.10.025.
Lu, S., Chen, Z.H., Xiang, Z.Q., Li, H., Li, H.M., Song, B., 2006. U-Pb ages of detrital zircons from the para-metamorphic rocks of the Qinling Group and their geological significance. Earth Sci. Front. 13, 303–310 (in Chinese with English abstract).
Ludwig, K.R., 2003. User's manual for Isoplot 3.00: a geochronological toolkit for Microsoft Excel.
Maniar, P.D., Piccoli, P.M., 1989. Tectonic discrimination of granitoids. Geol. Soc. Am. Bull. 101 (5), 635–643.
Mckeough, M., Lentz, D., Mcfarlane, C., Brown, J., 2013. Geology and evolution of pegmatite-hosted U-Th ± REE-Y-Nb Mineralization, Kulyk, Eagle, and Karin Lakes region, Wollaston Domain, northern Saskatchewan, Canada: examples of the dual role of extreme fractionation and hybridization processes. J. Geosci. https://doi.org/10.3190/jgeosci.153.
Mercadier, J., Annesley, I.R., McKechnie, C.L., Bogdan, T.S., Creighton, S., 2013. Magmatic and metamorphic uraninite mineralization in the Western Margin of the trans-hudson orogen (Saskatchewan, Canada): a uranium source for unconformity-related uranium deposits? Econ. Geol. 108, 1037–1065.
Middlemost, E.A., 1994. Naming materials in the magma/igneous rock system. Earth-Sci. Rev. 37 (3–4), 215–224.
Nex, P.A.M., Kinnaird, J.A., Oliver, G.J.H., 2001. Petrology, geochemistry and uranium mineralisation of post-collisional magmatism around Goanikontes, southern Central Zone, Damaran Orogen, Namibia. J. African Earth Sci. 33, 481–502. https://doi.org/10.1016/S0899-5362(01)00096-3.
No. 224 group of China National Nuclear Corporation, 2008. An internal report on the enrichment rules and prospect prediction of granite pegmatite-type uranium deposits in Dafeng area. Restricted data (in chinese).
Peiffert, C., Nguyen-Trung, C., Cuney, M., 1996. Uranium in granitic magmas: Part 2. Experimental determination of uranium solubility and fluid-melt partition coefficients in the uranium oxide-haplogranite-H2O-NaX (X = Cl, F) system at 770°C, 2 kbar. Geochim. Cosmochim. Acta 60, 1515–1529. https://doi.org/10.1016/0016-7037(96)00039-7.
Pelleter, E., Cheilletz, A., Gasquet, D., Mouttaqi, A., Annich, M., El Hakour, A., Féraud, G., 2007. Hydrothermal zircons: a tool for ion microprobe U-Pb dating of gold mineralization (Tamlalt–Menhouhou gold deposit—Morocco). Chem. Geol. 245 (3–4), 135–161.
Pettke, T., Audétat, A., Schaltegger, U., Heinrich, C.A., 2005. Magmatic-to-hydrothermal crystallization in the W-Sn mineralized Mole Granite (NSW, Australia): Part II: evolving zircon and thorite trace element chemistry. Chem. Geol. 220, 191–213. https://doi.org/10.1016/j.chemgeo.2005.02.017.
Plank, T., 2005. Constraints from Thorium/Lanthanum on Sediment Recycling at

Subduction Zones and the Evolution of the Continents. J. Petrol. 46, 921–944.
Qian, J.H., Yang, X.Q., Liu, L., Cao, Y.T., Chen, D.L., Yang, W.Q., 2013. Zircon U-Pb dating, mineral inclusions, Lu-Hf isotopic data and their geological significance of garnet amphibolite from Songshugou, North Qinling. Acta Petrol. Sin. 29, 3087–3098 (in Chinese with English abstract).
Qin, Z., Wu, Y., Siebel, W., Gao, S., Wang, H., Abdallsamed, M.I.M., Zhang, W., Yang, S., 2015. Genesis of adakitic granitoids by partial melting of thickened lower crust and its implications for early crustal growth: a case study from the Huichizi pluton, Qinling orogen, central China. Lithos 238, 1–12. https://doi.org/10.1016/j.lithos.2015.09.017.
Ratschbacher, L., Hacker, B.R., Calvert, A., Webb, L.E., Grimmer, J.C., McWilliams, M.O., Ireland, T., Dong, S., Hu, J., 2003. Tectonics of the Qinling (Central China): tectonostratigraphy, geochronology, and deformation history. Tectonophysics 366, 1–53. https://doi.org/10.1016/S0040-1951(03)00053-2.
Robb, L., 2004. Introduction to Ore-Forming Processes. Blackwell Publishing, Malden, MA, pp. 1–373.
Schaltegger, U., 2007. Hydrothermal Zircon. Elements 3, 51–79.
Scherer, E., Münker, C., Mezger, K., 2001. Calibration of the lutetium-hafnium clock. Science 293 (5530), 683–687.
Sha, Y.Z., Zuo, W.Q., Zhang, Z.S., Rao, C.J., 2011. Difference of ore-bearing and non-ore-bearing pegmatite in the Guangshigou area and its research significance. J. East China Inst. Technol. 34 (3), 215–223. https://doi.org/10.3969/j.issn.1674-3504.2011.03.003. in Chinese with English abstract.
Shi, Y., Yu, J.H., Santosh, M., 2013. Tectonic evolution of the Qinling orogenic belt, Central China: new evidence from geochemical, zircon U-Pb geochronology and Hf isotopes. Precambr. Res. 231, 19–60. https://doi.org/10.1016/j.precamres.2013.03.001.
Skirrow, R.G., Jaireth, S., Bastrakov, E.N., Schofield, A., Van Townsville Australia, 17-20 August 2009. Economic Geology Research Unit, James Cook University, Townsville, der W.S.E.B.T.-B.S.M. of the S. for G.A.T.M.D., 2009. Uranium mineral systems: Ore-forming processes and relationships among deposit types.
Skora, S., Blundy, J., 2010. High-pressure Hydrous Phase Relations of Radiolarian Clay and Implications for the Involvement of Subducted Sediment in Arc Magmatism. J. Petrol. 51, 2211–2243.
Stone, M., 2000. Petrogenetic implications from biotite compositional variations in the Cornubian granite batholith. Mineral. Mag. 64 (4), 729–735.
Stepanov, A., Mavrogenes, A.J., Meffre, S., Davidson, P., 2014. The key role of mica during igneous concentration of tantalum. Contrib. Mineral. Petrol. 167, 1009. https://doi.org/10.1007/s00410-014-1009-3.
Stepanov, A.S., Hermann, J., Rubatto, D., Rapp, R.P., 2012. Experimental study of monazite/melt partitioning with implications for the REE, Th and U geochemistry of crustal rocks. Chem. Geol. 300–301, 200–220. https://doi.org/10.1016/j.chemgeo.2012.01.007.
Sun, S.S., McDonough, W.F., 1989. Chemical and isotopic systematics of oceanic basalts: implications for mantle composition and processes. Geol. Soc. London Spec. Publ. 42, 313–345.
Tang, Z.L., 2002. Metallogenic System and Metallogenic Tectonic Dynamics for Sourthwest Fringe of North China Ancient land (longshoushan- Qilianshan). Geological Publishing House, Beijing.
Tischendorf, G., Forster, H.J., Gottesmann, B., Rieder, M., 2007. True and brittle micas: composition and solid-solution series. Mineral. Mag. https://doi.org/10.1180/minmag.2007.071.3.285.
Tischendorf Gerhard, Hans-Jürgen, F., Bärbel, G., 1999. The correlation between lithium and magnesium in trioctahedral micas: improved equations for Li2O estimation from MgO data. Mineral. Mag. https://doi.org/10.1180/002646199548312.
Vervoort, J.D., Blichert-Toft, J., 1999. Evolution of the depleted mantle: Hf isotope evidence from juvenile rocks through time. Geochim. Cosmochim. Acta 63, 533–556. https://doi.org/10.1016/S0016-7037(98)00274-9.
Vervoort, J.D., Jonathan Patchett, P., 1996. Behavior of hafnium and neodymium isotopes in the crust: constraints from Precambrian crustally derived granites. Geochim. Cosmochim. Acta 60, 3717–3733. https://doi.org/10.1016/0016-7037(96)00201-3.
Wan, J., Gao, L.B., Wang, L.X., 1992. Metallogenic environmental study and prospect assessment of tile granite-pegmatite-type uranium deposit in shangxian-danfeng triangle area, shaanxi. Uranium Geol. 5, 257–263 (in Chinese with English abstract).
Wang, H., Wu, Y.-B., Gao, S., Liu, X.-C., Liu, Q., Qin, Z.-W., Xie, S.-W., Zhou, L., Yang, S.-H., 2013a. Continental origin of eclogites in the North Qinling terrane and its tectonic implications. Precambrian Res. 230, 13–30.
Wang, J.B., Hou, X.H., Li, W.H., Zhang, L., Zhao, Y.D., Chen, H.B., Li, W.H., 2018. The metallogenic characteristics and metallogenic model of the pegmatite type uranium deposit in Danfeng Area, Eastern Qinling Mountains. Earth Sci. 42, 1–16 (in Chinese with English abstract).
Wang, T., Wang, X., Tian, W., Zhang, C., Li, W., Li, S., 2009. North Qinling Paleozoic granite associations and their variation in space and time: implications for orogenic processes in the orogens of central China. Sci. China Ser. D Earth Sci. 52, 1359–1384. https://doi.org/10.1007/s11430-009-0129-5.
Wang, X., Wang, T., Zhang, C., 2013b. Neoproterozoic, Paleozoic, and Mesozoic granitoid magmatism in the Qinling Orogen, China: Constraints on orogenic process. J. Asian Earth Sci. 72, 129–151.
Ward, R., Stevens, G., Kisters, A., 2008. Fluid and deformation induced partial melting and melt volumes in low-temperature granulite-facies metasediments, Damara Belt, Namibia. Lithos 105, 253–271. https://doi.org/10.1016/j.lithos.2008.04.001.
Wiedenbeck, M., Allé, P., Corfu, F., Griffin, W.L., Meier, M., OberlI, F., Quadt, A.V.O.N., Roddick, J.C., Spiegel, W., 1995. Three natural zircon standards For U-Th-Pb, Lu-Hf, trace element and Ree Analyses. Geostand. Newsl. 19, 1–23. https://doi.org/10.1111/j.1751-908X.1995.tb00147.x.
Wu, F.Y., Yang, Y.H., Xie, L.W., Yang, J.H., Xu, P., 2006. Hf isotopic compositions of the standard zircons and baddeleyites used in U-Pb geochronology. Chem. Geol. 234, 105–126. https://doi.org/10.1016/j.chemgeo.2006.05.003.
Wu, Y.B., Hanchar, J.M., Gao, S., Sylvester, P.J., Tubrett, M., Qiu, H.-N., Wijbrans, J.R., Brouwer, F.M., Yang, S.-H., Yang, Q.-J., Liu, Y.-S., Yuan, H., 2009. Age and nature of eclogites in the Huwan shear zone, and the multi-stage evolution of the Qinling-Dabie-Sulu orogen, central China. Earth Planet. Sci. Lett. 277, 345–354. https://doi.org/10.1016/j.epsl.2008.10.031.
Wu, Y.B., Zheng, Y.F., 2013. Tectonic evolution of a composite collision orogen: an overview on the Qinling–Tongbai–Hong'an–Dabie–Sulu orogenic belt in central China. Gondwana Res. 23, 1402–1428. https://doi.org/10.1016/j.gr.2012.09.007.
Xing, L., Trail, D., Watson, E.B., 2013. Th and U partitioning between monazite and felsic melt. Chem. Geol. 358, 46–53. https://doi.org/10.1016/j.chemgeo.2013.07.009.
Yan, Q.R., Wang, Z.Q., Yan, Z., Xiang, Z.J., Wang, T., Zhang, H.Y., 2009. Tectonic affinity and timing of two types of amphibolites within the Qinling Group, north Qinling orogenic belt. Acta Petrol. Sin. 25, 2177–2194 (in Chinese with English abstract).
Yang, J., Xu, Z., Dobrzhinetskaya, L.F., Green, H.W., Pei, X., Shi, R., Wu, C., Wooden, J.L., Zhang, J., Wan, Y., Li, H., 2003. Discovery of metamorphic diamonds in central China: an indication of a > 4000-km-long zone of deep subduction resulting from multiple continental collisions. Terra Nov. 15, 370–379. https://doi.org/10.1046/j.1365-3121.2003.00511.x.
Yang, L., Fukun, C., Yi-Zeng, Y., Shuang-Qing, L., Zhu, X.Y., 2010. Zircon U-Pb ages of the Qinling Group in Danfeng area: recording Mesoproterozoic and Neoproterozoic magmatism and Early Paleozoic metamorphism in the North Qinling terrain. Acta Geol. Sin. 26, 1589–1603 (in Chinese with English abstract).
Yu, H., Zhang, H.F., Li, X.H., Zhang, J., Santosh, M., Yang, Y.H., Zhou, D.W., 2016. Tectonic evolution of the North Qinling Orogen from subduction to collision and exhumation: evidence from zircons in metamorphic rocks of the Qinling Group. Gondwana Res. 30, 65–78. https://doi.org/10.1016/j.gr.2015.07.003.
Yuan, F., Liu, J.J., Carranza, E.J.M., Zhang, S., Zhai, D.-G., Liu, G., Wang, G.-W., Zhang, H.-Y., Sha, Y.-Z., Yang, S.-S., 2018. Zircon trace element and isotopic (Sr, Nd, Hf, Pb) effects of assimilation-fractional crystallization of pegmatite magma: a case study of the Guangshigou biotite pegmatites from the North Qinling Orogen, central China. Lithos 302–303, 20–36. https://doi.org/10.1016/j.lithos.2017.12.022.
Zhai, X., Day, H.W., Hacker, B.R., You, Z., 1998. Paleozoic metamorphism in the Qinling orogen, Tongbai Mountains, central China. Geology 26, 371–374 (in Chinese with English abstract).
Zhang, C., Liu, L., Wang, T., Wang, X., Li, L., Gong, Q., Li, X., 2013. Granitic magmatism related to early Paleozoic continental collision in North Qinling. Chinese Sci. Bull. 58 (35), 4405–4410.
Zhang, G.W., 1988. Formation and Evolution of the Qinling Orogen. Northwest University Press, Xi'an, pp. 1–192 (in Chinese with English abstract).
Zhao, K.-D., Jiang, S.-Y., Ling, H.-F., Palmer, M.R., 2014. Reliability of LA-ICP-MS U-Pb dating of zircons with high U concentrations: a case study from the U-bearing Douzhashan Granite in South China. Chem. Geol. 389, 110–121. https://doi.org/10.1016/j.chemgeo.2014.09.018.
Zeng, L.J., Jin, J.F., 1994. Discussion on the migration and precipitation mechanism of the uranium in some granite-pegmatite type uranium deposit. J. East China Geol. Inst. 17 (03), 264–269 (in Chinese with English abstract).
Zheng, Y.F., Xia, Q.X., Chen, R.X., Gao, X.Y., 2011. Partial melting, fluid supercriticality and element mobility in ultrahigh-pressure metamorphic rocks during continental collision. Earth Sci. Rev. 107, 342–374. https://doi.org/10.1016/j.earscirev.2011.04.004.
Zhu, X.K., O'Nions, R.K., 1999. Zonation of monazite in metamorphic rocks and its implications for high temperature thermochronology: a case study from the Lewisian terrain. Earth Planet. Sci. Lett. 171, 209–220. https://doi.org/10.1016/S0012-821X(99)00146-6.
Zuo, W., Sha, Y., Chen, B., Luo, Z., Zhang, Z., 2010. U-Pb isotopic dating of zircon from damaogou granite stock of Guangshigou uranium deposit in Danfeng area and it's significance. Uranium Geol. 26 (4), 222–227 (in Chinese with English abstract).